A Theoretical Investigation of the Ability of Magnetic Miniature Robots to Exert Forces and Torques for Biomedical Functionalities

Yuxuan Xiang, and Jiachen Zhang

***Abstract*—Magnetic miniature robots exert forces and torques onto the environment to conduct minimally invasive diagnostic and therapeutic tasks. The orders of magnitude of forces and torques determine what functionalities these robots can achieve. Although some studies have been dispersedly reported, the forces and torques have yet to be systematically investigated within biomedical context from underlying physical principles, leaving their theoretical limits elusive. This work constructs a theoretical framework from governing equations to calculate the forces and torques exerted by magnetic miniature robots in their respective targeted workspace to achieve functionalities. It reports that the existing miniature robots with a maximum characteristic length of 10^{-2} m can exert a force and a torque up to the order of 10^{-1} N and 10^{-2} Nm, respectively, considering realistic actuation paradigms and constraints. The attainable force and torque magnitudes are on par with the requirements of surgeries at human head (e.g., brain, eyes, and ears surgeries) or within adjacent regions of human skin (e.g., surgeries in the bladder and some blood vessels), as well as the surgeries on small animals. But they are insufficient for operations in deep-buried regions of large animals and human (e.g., implant therapy, biopsy, and tissue removal). Hence, potential strategies to further raise the ceiling of the ranges are examined to extend the functionality catalog and expand the operating scope of these robots.**

***Index Terms*—Magnetic actuation, miniature robots, medical and surgical robots.**

I. Introduction

MINIATURE robots have characteristic length values at the millimeter, micrometer, and nanometer scale, which are termed as the millirobots, microrobots, and nanorobots, respectively. They have attracted significant interest due to their entrancing applications in various fields, especially in minimally invasive healthcare and biomedical engineering [1]. Among the different miniature robots working with a large variety of actuation strategies, the robots that are actuated and controlled by an externally applied magnetic field stand out thanks to the magnetic field's advantageous capabilities of penetrating biological substances and simultaneously exerting both forces and torques. These remotely controlled magnetic robots have dramatically different working principles with traditional lager robots. Nevertheless, they still conduct tasks and achieve functionalities in a similar manner: by exerting forces and torques to the environments as illustrated by the examples in Fig. 1. Thus, the force and torque exerted by these robots play a prominent role in executing tasks.

However, there has yet to be a systematic and quantitative investigation of what orders of force and torque magnitude these robots can theoretically achieve, considering their various geometries, materials, and peripherals. A previous discussion on magnetic methods in robotics [2] focused on general governing equations but did not provide with an intuitive understanding of the force and torque capabilities of specific miniature robot systems. Actually, only scattered and isolated reports on the values or ranges of the forces and torques exist in the literature [3], [4]. How these reported numbers compare with each other has not been discussed, especially within the context of targeted applications. For these robots to move beyond proof-of-concept and become applicable to real-world tasks, their capable ranges of forces and torques need to be quantitatively identified and the approaches to raise the upper limit need to be examined.

This letter theoretically investigates the forces and torques that magnetic miniature robots can output to achieve functionalities using available hardware systems. We build a mathematical framework, which is broadly applicable to existing magnetic miniature robots, to analyze the physical laws that govern their working principles and to calculate the order of magnitude of their mechanical interaction with the workspace. Parameters of existing robotic systems are gathered from the literature to define the scope of our discussion, e.g., robot characteristic lengths, magnetizations, and external field generators. Results from our developed

Manuscript received: October 28, 2022; Revised: January 9, 2023; Accepted: January 25, 2023. This paper was recommended for publication by Editor Pietro Valdastri upon evaluation of the Associate Editor and Reviewers' comments. This work was supported by the City University of Hong Kong under Grant No. 9610539. *(Corresponding author: Jiachen Zhang.)*

Yuxuan Xiang and Jiachen Zhang are with the Department of Biomedical Engineering, City University of Hong Kong, Hong Kong SAR, China (e-mail: yxxiang.bme@my.cityu.edu.hk; jzhang.bme@cityu.edu.hk).

This letter has supplementary downloadable material available at http://ieeexplore.ieee.org, provided by the author. The supplementary material for additional information on the analysis results of permanent magnets and electromagnetic coils as the field generator, and detailed table that collected parameters from previously reported magnetic miniature robotic systems.

Color versions of one or more of the figures in this article are available online at http://ieeexplore.ieee.org

Digital Object Identifier (DOI): see top of this page.

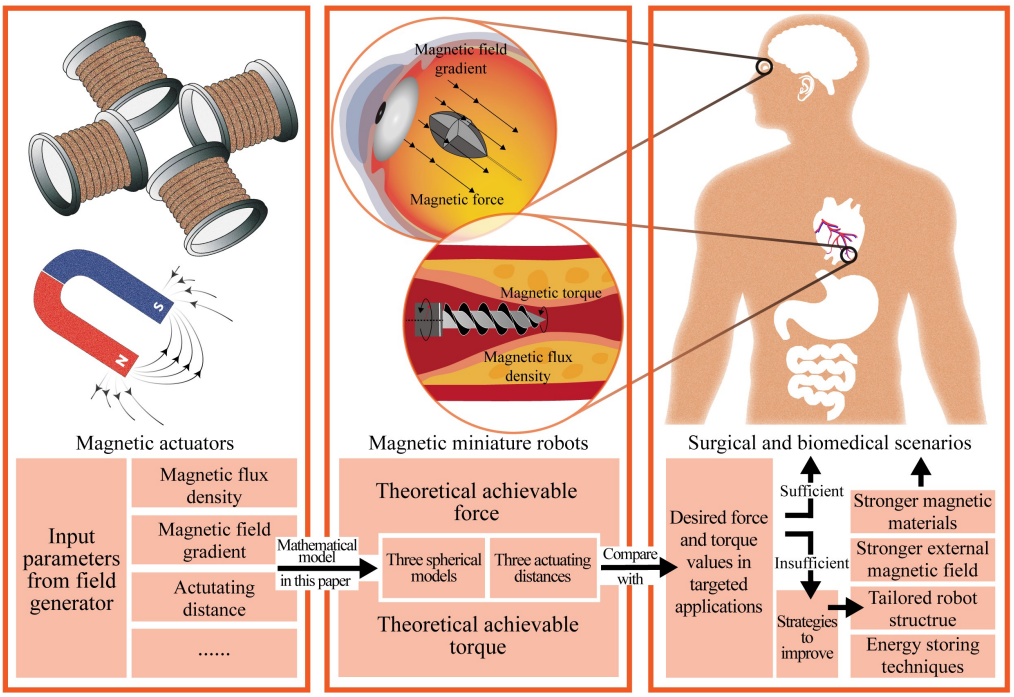

Fig. 1. A schematic illustrating the methodology and contribution of this work. Parameters from the field generators and magnetic miniature robots are imported to our model to theoretically demonstrate the attainable maximum magnetic force and torque outputs. Potential improvement strategies are discussed if these values are insufficient in targeted applications. Ultimately, magnetic miniature robots with sufficient force and torque output are able to accomplish specific tasks in medical scenarios (e.g., retinal drug delivery [19], thrombus removal [62], etc.).

theoretical framework are juxtaposed with the measurement and experimentally observed phenomena from preceding studies, showing an evident agreement between each other in the order of magnitude and the scaling trend. The calculated values are then compared against the required force and torque values of targeted biomedical operations, identifying the potentials as well as the incompetence of these robots in real-world tasks. Finally, possible approaches to uplift the ceiling of the forces and torques are discussed.

II. Theoretical Model

A miniature robot obtains its magnetism using onboard magnetic materials that are either embedded in its body or coated on its surface. An external magnetic field interacts with these onboard magnetic parts and thus exerts forces and torques on the robot. Subsequently, these forces and torques are transferred to the workspace environment by manipulating the robot as an end-effector of the whole robotic system to perform tasks. Various types of magnetic materials have been employed in miniature robots to accommodate different applications. Among them, neodymium-iron-boron (NdFeB) is widely employed to endow miniature robots with magnetic properties due to its superior magnetic properties with a high remanence [5] and affordable price [6].

Since miniature magnetic robots are mostly placed in a magnetic field that is orders of magnitude larger in dimension, a robot can be effectively simplified as a magnetic dipole, which is a hypothetical point model with zero volume and a non-zero magnetic moment. Here, we denote the magnetic moments of the robot and the external magnetic field generator as $\mathbf{m_1}$ and $\mathbf{m_2}$, respectively. The external magnetic field, denoted by the field flux density $\mathbf{B_2}$, is generated by a single or multiple permanent magnets, or an electromagnet system with a single or multiple coils. The magnetic moment of a permanent magnet can be calculated as:

$$\mathbf{m_2} = \iiint \mathbf{M_2} dV \tag{1}$$

where $\mathbf{M_2}$ is the magnet's magnetization and dV is the infinitesimal volume element. Equation (1) for a magnet with homogeneous magnetization is simplified as:

$$\mathbf{m_2} = \mathbf{M_2} V_m \tag{2}$$

where V_m is the total magnet volume. For magnetic dipoles, current loop and magnetic charge are both natural and available models for analyzing [7]. Considering a single solenoid in electromagnet, its magnetic moment is calculated using the current loop model as:

$$\mathbf{m_2} = nI\mathbf{S} \tag{3}$$

where n is the number of turns of wire in the electromagnetic coil, I is the current, and $\mathbf{S}$ is the vector area of the loop. Considering a current loop with a radius R and a distance to robot r, (3) is only valid when $R \ll r$ [8]. Previous

studies have reported various custom-built electromagnetic coil systems consisting of a varying number of coils for different purposes. These preceding research only reported magnetic flux density at workbench center and its changing frequency, without giving much of other details. Thus, this letter does not attempt to establish a general and systematic model for various electromagnets. Instead, we restrain the discussion to single electromagnetic coil as the source and consider it as a magnetic dipole $\mathbf{m_2}$, which has been reported to be a suitable approach to analyze the magnetic field of a popular electromagnet OctoMag [9]. OctoMag demonstrates a magnetic moment of 4.51 Am^2 for an upper magnet and 8.18 Am^2 for a lower magnet through data fitting using a finite-element-method (FEM) model. To avoid confusion, it should be noted that a single electromagnetic coil could still have multiple turns of the wire, i.e., $n \geq 1$. The magnetic force imparted to $\mathbf{m_1}$ by $\mathbf{m_2}$ is calculated by (4) and (5), based on the current loop model and magnetic charge model, respectively.

$$\mathbf{F}_{21} = \nabla \left(\mathbf{m}_1 \cdot \mathbf{B}_2 \right) \tag{4}$$

$$\mathbf{F}_{21} = \left(\mathbf{m}_1 \cdot \nabla \right) \mathbf{B}_2 \tag{5}$$

If there are no electrical currents or time-varying electrical fields in the system, (4) and (5) are equivalent since both $\nabla \times \mathbf{B_2}$ and $\nabla \cdot \mathbf{B_2}$ are zero. $\mathbf{B_2}$ is generated by $\mathbf{m_2}$ and can be calculated using (6) identically for both current loop and magnetic charge models as:

$$\mathbf{B}_2 = \frac{\mu_0}{4\pi} \left[\frac{\mathbf{3r} \left(\mathbf{r} \cdot \mathbf{m}_2 \right)}{r^5} - \frac{\mathbf{m}_2}{r^3} \right] \tag{6}$$

where $\mu_0 = 4\pi \times 10^{-7}$ H/m is the vacuum permeability, $\mathbf{r}$ is the distance vector between dipole model center of robot and external magnet and r is the distance. Additionally, the magnetic force exerted by the external magnetic source $\mathbf{m_2}$ on the magnetic robot $\mathbf{m_1}$ can also be expressed as:

$$\mathbf{F}_{21} = \frac{3\mu_0}{4\pi r^5} \left[\begin{array}{l} \left(\mathbf{m}_2 \cdot \mathbf{r} \right) \mathbf{m}_1 + \left(\mathbf{m}_1 \cdot \mathbf{r} \right) \mathbf{m}_2 + \\ \left(\mathbf{m}_1 \cdot \mathbf{m}_2 \right) \mathbf{r} - \frac{5(\mathbf{m}_2 \cdot \mathbf{r})(\mathbf{m}_1 \cdot \mathbf{r})}{r^2} \mathbf{r} \end{array} \right] \tag{7}$$

$$\boldsymbol{\tau}_{21} = \mathbf{m}_1 \times \mathbf{B}_2 \tag{8}$$

Meanwhile, the magnetic torque exerted by $\mathbf{m_2}$ to $\mathbf{m_1}$ is obtained directly through (8). However, for miniature robots composed of hard-magnetic soft active materials (hmSAMs), magnetic particles embedded in a soft matrix cannot transmit magnetic torque from the external magnetic field to the robot body without loss, due to the particle's local rotation within the base matrix. Therefore, the torque transmission efficiency η needs to be considered by (9) [10]:

$$\eta = \cos \left\{ \frac{\pi}{2} \left(1 - \frac{\pi}{2} f \right) \left[1 - \exp \left(-0.165 \frac{M_1 B_2}{G} \right) \right] \right\} \tag{9}$$

$$\tau_{21}^m = \eta \tau_{21}^p \tag{10}$$

where f is volume fraction of magnetic particles, M_1 is the magnetization of the magnetic particles, and G is shear modulus of soft matrix. Total magnetic torque outputs τ_{21}^m of magnetic robot with soft matrix can be calculated by (10), where τ_{21}^p is the total magnetic torque on particles.

TABLE I
THREE DIFFERENT WORKING DISTANCES r

Distance r	Targeted application scenarios
50 mm	*In vitro* applications, small animals (e.g., mice and rabbits), microscale operations (e.g., cell manipulation)
100 mm	Human head (e.g., brain, eyes, cochlea), adjacent regions to skin (e.g., bladder and some blood vessels)
200 mm	Deep-buried regions like abdomen (e.g., heart, intestines), surgeries involving torso

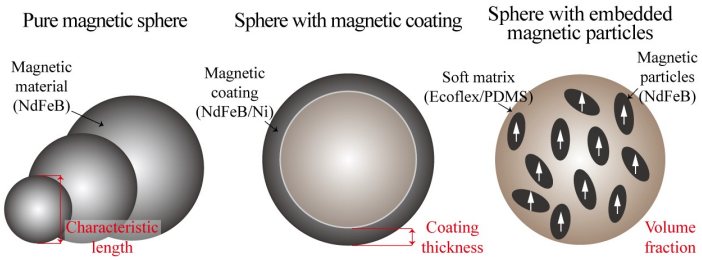

Fig. 2. A schematic showing the three calculation models employed in the developed framework for magnetic miniature robots.

III. METHODOLOGY

Previous studies that have reported force or torque data applied to miniature magnetic robots are summarized in Table S1. Comparison of the ability to generate magnetic field between permanent magnets and electromagnets are presented in SM-S1. Considering the more superior magnetic properties of permanent magnets, their abilities to generate magnetic field have been transformed into the same distance (i.e., 200 mm) and have been compared through the dipole model in SM-S2 and Table S2. The result shows a non-custom N52-grade cuboidal NdFeB magnet, which has a 50 mm side length with a magnetic moment of $\mathbf{m_2}$= 131 Am^2 and an ability to generate a magnetic field with $\mathbf{B_2}$= 3.28 mT and $\nabla \mathbf{B_2}$= 49.13 mT/m at 200 mm, is the most ideal external field generator for this work considering customized cost and dipole model error. Thus, this magnet is selected as the external magnetic field generator to calculate the theoretical maximum forces and torques.

Miniature magnetic robots have been reported to work in various biomedical scenarios with different working distances, ranging from 8 mm to 240 mm. It is pointless and inconsequential to evaluate the performance only at one specific distance due to the fact that magnetic force and torque outputs decrease exponentially with the distance. Hence, we propose to use three levels of working distances r [11] to evaluate different potential applications in Table I. Here, we consider different sizes of the organ and the distances from specific organ to skin surface. This application-oriented classification ensures that the varying working distances of robots are always greater than 1.5 radii of the minimum bounding sphere, which constrains the error of dipole model to below 2% [12].

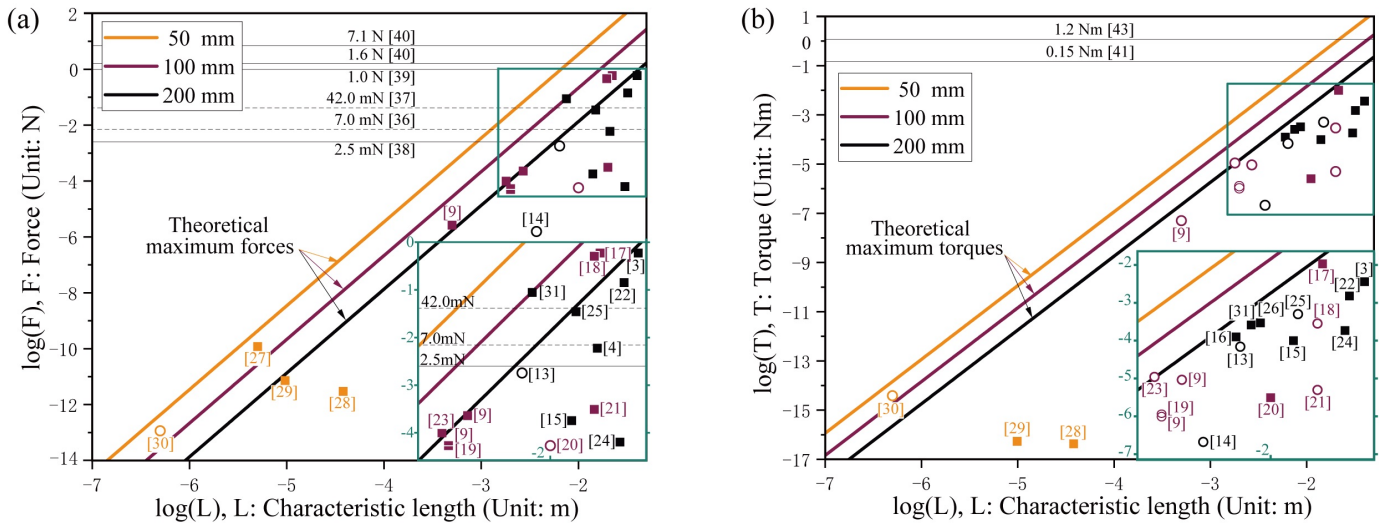

Fig. 3. Comparisons between theoretically achievable forces (a) and torques (b), reported values from previous studies, and desired maximum and minimum values by various biomedical applications. Upper limits in specific medical applications have been labelled by dashed lines, while lower limits shown as solid lines determine minimum required forces or torques to be applied. Previously reported force and torque data are marked out to show their potential improvement and capable application scenarios. Solid cubes refer to reported data, while hollow circles refer to calculated data using the proposed dipole model with known parameters.

Meanwhile, the ability of a magnetic miniature robot with spherical geometry to exert force and torque is calculated. The sphere is selected attributed to its isotropic geometry which ensures an equivalent characteristic length in all directions without causing significant deviations to force and torque outputs of robots at the same characteristic length. As illustrated in Fig. 2, the proposed model generalizes previously reported magnetic miniature robots with different magnetized bodies in three categories: pure magnetic sphere, sphere with magnetic surface coating, and sphere with embedded magnetic particles. Magnetic miniature robots can be either fully magnetic (Category 1) or composed of both magnetic parts and non-magnetic parts (Category 2 and 3) [63], [64], which can simultaneously have multiple parts described in these models. More specifically, Category 1 represents various miniature robots that are completely composed of magnetic materials. Category 2 represents various rigid-bodied magnetic robots with a magnetic coating and non-magnetic core [28], [65]. Category 3 represents various soft-bodied magnetic robots with embedded magnetic materials [13], [34].

In our model, the magnetic moment of the robot $\mathbf{m_1}$ is assumed to be across the geometric center of the evaluated sphere, simultaneously align with the direction of the external magnetic field $\mathbf{B_2}$ when considering maximum force, while $\mathbf{m_1}$ is assumed to be orthogonal with $\mathbf{B_2}$ when considering maximum torque. The theoretical maximum magnetic forces and torques applied on the spherical, generalized robot models with various characteristic lengths are simulated through custom-built MATLAB codes with external permanent magnet placed at three distances, i.e., 50 mm, 100 mm, and 200 mm.

IV. Results and Discussions

A. Pure Magnetic Sphere Model

In Category 1, the results are shown in Fig. 3 and compared with the reported data from representative previous research. Previous miniature robots are designed with various geometric shapes, including swimmer [13], [14], helical screw [15], [16], capsule [3], [17], [18], needle [9], [19], catheter [20], [21], cylinder [22], [23], coil [24], gripper [4], scissor [25], spring [26], bead [27], bacteria flagella [28], [29], swarm [30], and bio-inspired structure [31] with a characteristic length L ranging from 500 nm to 40 mm. The comparison between the reported data points and the calculated theoretical limits shows an evident agreement between each other in the order of magnitude and the scaling trend, validating the proposed theoretical framework. The outliers of the reported data points that are above the theoretical maximum are attributed to an overly short working distance (e.g., 8 mm) utilized in experiments or simulations [31].

B. Magnetic Coated Sphere Model

In Category 2, the capable magnetic forces and torques of spherical miniature robots of a non-magnetic core and a magnetic coating surface have been calculated with varying coating thickness in Fig. 4. By considering both NdFeB and Nickel (M_{Ni} ≈257 kA/m [32]) coatings of a sphere with a 1 mm diameter at a working distance of 50 mm, the results show a relatively smaller range of generating torque and force compared with a maximum theoretical force of 10^{-3} N and torque of 10^{-4} Nm from a pure magnetic sphere of 1 mm diameter. Under the field generated by a permanent magnet, the results from our model suggest that this sphere with a

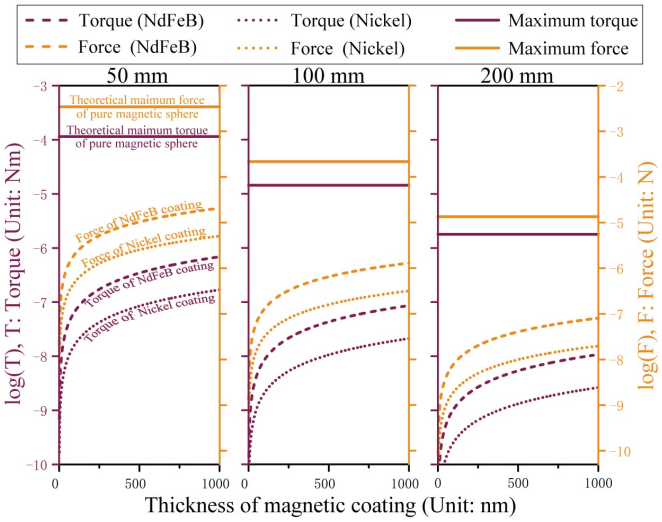

Fig. 4. Theoretical maximum force and torque that can be generated by NdFeB- and Ni-coated robots with varying coating thickness. The spherical body has a diameter of 1 mm and is actuated at working distances of 50 mm, 100 mm, and 200 mm.

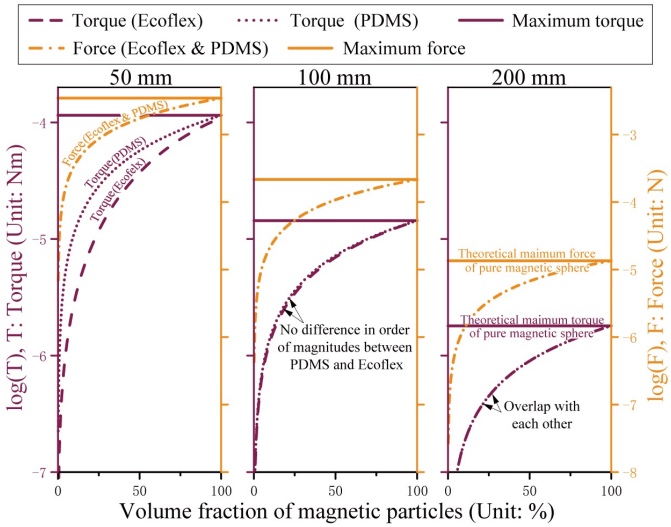

Fig. 5. Theoretical maximum torque and force that can be generated by soft robots embedded with NdFeB particles with varying volume fraction. The spherical body has a diameter of 1 mm and has been actuated at three levels working distance. At a relatively short working distance, soft matrix made of PDMS tend to produce higher magnetic torque than Ecoflex. When working distance increase up to 200 mm, no significant difference can be observed.

1 μm NdFeB coating can theoretically exert 10^{-5} N force and 10^{-7} Nm torque, 10^{-6} N force and 10^{-8} Nm torque, and 10^{-8} N force and 10^{-8} Nm torque at 50 mm, 100 mm, and 200 mm distances, respectively. Compared with NdFeB coating, Ni-coated magnetic sphere suffers from smaller magnetization and thus exhibit weaker magnetic forces and torques output. Here, we only theoretically investigate the achievable maximum forces and torques of these coated robots. Specific constrains have to be considered in real-world applications: for example, Ni layer cannot retain its magnetization direction under magnetic field above 20 mT [33].

C. Magnetic Particles Embedded Sphere Model

For Category 3, a soft spherical matrix embedded with NdFeB magnetic particles with varying particles volume fractions f is tested. To evaluate the maximum magnetic torque outputs, torque transmission efficiency η is applied to consider the local particle rotation relative to the soft matrix by (9) and (10). Such soft magnetic robots have been frequently reported in previous research. Both Ecoflex (G ≈15 kPa) and poly-dimethylsiloxane (PDMS, G ≈250 kPa) are widely used soft materials and are compared at different levels of working distances as shown in Fig. 5. Considering a frequently reported large volume fraction of 27.56% (mass ratio of 3:1, for NdFeB particles to PDMS) from previous literature [34], this soft sphere with 1 mm diameter can attain 10^{-4} N force and 10^{-5} Nm torque at 50 mm, 10^{-5} N force and 10^{-6} Nm torque at 100 mm, and 10^{-6} N force and 10^{-7} Nm torque at 200 mm. Soft miniature robots composed of Ecoflex demonstrate a slightly lower torque transmission efficiency η due to lower shear module G compared with PDMS-based soft robots. However, this gap dramatically reduces with the increase of working distance and the results show no differences in the orders of torque magnitudes for 100 and 200 mm.

In summary, the evaluations of both surface coated model (Category 2) and embedded particles model (Category 3) show relatively weaker ability to exert forces and torques due to their smaller volume of onboard magnetic parts compared with pure magnetic body (Category 1) at the same characteristic length L and working distance r. These magnetic forces and magnetic torques are $\propto L^{-3}$ and $\propto r^{-4}$, $\propto L^{-3}$ and $\propto r^{-3}$, respectively. Results from Fig. 3 suggest that the reported miniature robots with a maximum characteristic length at the order of 10^{-2} m have the ability to exert a maximum force at the order of 10^{-1} N and a maximum torque at the order of 10^{-2} Nm, which have been reported to be relevant in various applications [3], [17], [18], [22].

V. Force and Torque Requirements in Targeted Biomedical Applications

Considering real-world constrains in these applications, different clinical scenarios pose strict requirements for not only the upper limit but also the lower limit of physical quantities. It is shown that 75% of all tool and tissue interaction forces during vitreoretinal surgery are below 7.5 mN [35], while beyond 7 mN it is likely to cause retinal breaks and tears [36]. During cochlear implantation, the threshold for undesired puncturing of the basilar membrane was measured to be approximately 42 mN [37].

The above upper limits of force are achievable and controllable through adjusting magnetic materials and working distance, but specific lower limits of some clinical applications

still pose a challenge for current miniature robots. Minimum puncturing forces in tissue penetration were measured to be 2.5 mN for mouse brain [38] and up to 1.0 N for porcine tissue [39]. Meanwhile, tissue cutting forces using the Metzenbaum scissors were studied for rat and sheep tissues with 1.6 N and 7.1 N for liver, 7.0 N and 17.5 N for skin, respectively [40]. Similar minimum insertion torque requirement has to be considered during implant therapy like osseointegration. It has been experimentally demonstrated that an insertion torque of 0.15 Nm is needed to maintain the stability for immediately loaded implants after 3 years of loading [41]. Limited by fracture and deformation during a cutting action, soft object like potatoes with a Young's modulus of 2 MPa (similar to human cartilage with a modulus of 1.76 MPa [42]) require a cutting torque of approximately 1.2 Nm [43].

Considering limited operating space and long working distance for deep-buried biomedical application workspace, desired forces and torques in the aforementioned biomedical applications are difficult to achieve. Currently attainable forces and torques of pure magnetic miniature robots are on par with the requirements in surgeries at human head (e.g., brain, eyes, and ears) as well as tissue penetration for small animals. Meanwhile, magnetic force and torque is $\propto r^{-4}$ and $\propto r^{-3}$, respectively. With relatively short actuating distance, these values are theoretically sufficient in minimally invasive surgeries involving organs and tissues in the vicinity of skin surface (e.g., the bladder [44], [45] and some blood vessels [46]). However, current miniature robots can hardly be operated in deep-buried regions of large mammals and human surgery (e.g., implant therapy, biopsy, and tissue removal) because the working distance is inevitably longer. Therefore, potential strategies to further raise the ceiling of force and torque ranges are discussed to extend the functionality catalog of these robots.

VI. Improvement Strategies

Enhanced NdFeB materials [6], [47]–[49] and other magnetic materials [50]–[52] result in a larger $\mathbf{m_2}$, while more powerful external magnetic field generator results in a larger $\mathbf{B_2}$. For example, magnetic resonance imaging (MRI) systems with significantly higher field strengths of 1.5 T, 3 T and 7 T [53] have the potential to increase the theoretical maximum magnetic torque by 1-2 orders of magnitude. Meanwhile, traditional magnetic field generators such as customized large permanent magnets [20] and clinical-scale electromagnetic coil systems [54] are also capable of generating larger forces and torques. A previous reported microscissor with a characteristic length of 15 mm using the latter coil system can exert 1.5 N force, which shows a 42.9-fold increase and can be potentially applied for rat liver cutting [25].

Miniature robots with special structures have been reported to exert larger forces or torques [55]–[57]. Previous research demonstrated that a twisted helical microrobot with chemically etched sharp tip [55] and micro drilling device with blades [56] have promising performance in penetrating mouse liver lobe and thrombus, respectively. A recent report showed that a robot with a characteristic length of 3 mm functioned as a torque amplifier (from 1.85 μNm to 0.182 mNm with a 97.4-fold increase) attributed to its gearbox structure [57]. Furthermore, assembling magnetic particles into chains can generate unit specific torques of 68 ± 2 Nm/kgT which is significantly higher than the value of silicone cantilevers with unchained iron oxide nanoparticles (0.9 Nm/kgT) [58].

Energy storing and releasing adds extra amount into the energy reservoir at the robot's disposal to generate larger forces and torques. Recent studies suggested elastic potential energy of spring [44] and energy induced by phase change-based volumetric inflation [59] can potentially raise the force output of miniature robots to the order of 10^0-10^1 N. Similar energy-based methodologies suggested a drilling device using torsional actuation of the coiled muscle can release the energy stored in a pre-stretched elastomer and can be employed as an amplifier from 149 μNm to $\sim$1.2 mNm for torque and 1 N to 14 N for force [60]. Additionally, an impact force-based needle converts kinetic energy into mechanical energy and generates 410 mN penetration force, showing 22.7-fold increase in force with a more than 20 times smaller volume [61].

These aforementioned miniature robots employing stronger magnetic materials, applying stronger external magnetic field, tailoring robot structure, and implementing energy storing techniques can potentially exert higher force and torque for demanding biomedical procedures, which previous miniature robots with size of the same order of magnitude are not capable of.

VII. Conclusion

This letter constructs a theoretical framework from underlying working principles that is broadly applicable to magnetic miniature robots to calculate their forces and torques in targeted workspace with existing setups. The calculated theoretical limits by the proposed framework show an evident agreement in comparison with previously reported data in terms of the order of magnitude and the scaling trend, validating its accuracy. Magnetic miniature robots with various characteristic lengths (ranging from 10^{-7} to 10^{-2} m), magnetic configurations (pure magnetic body, surface-coated body, and particles embedded body), and peripheral field generators (permanent magnets or electromagnetic coil systems) are investigated and evaluated. Considering available actuation paradigms and practical constraints, attainable forces and torques of these miniature robots are insufficient for operations in deep-buried regions of large mammals and human surgery (e.g., implant therapy, biopsy, and tissue removal). Therefore, potential strategies using powerful external magnetic field, tailored robot structure, implementation of energy storing and releasing techniques, and enhanced magnetic materials, to further raise the ceiling of capable magnetic force and torque ranges are discussed

to theoretically extend the functionality catalog of miniature robots.

This study lays a theoretical foundation for researchers to understand the force- and torque-outputting capability of existing and upcoming magnetic miniature robots and thus help them obtain an intuitive idea of what functionalities are possible for different distinct designs, while at the same time pointing out the directions of potential improvement.

REFERENCES

[1] J. Li, B. E.-F. de Ávila, W. Gao, L. Zhang, and J. Wang, "Micro/nanorobots for biomedicine: Delivery, surgery, sensing, and detoxification," *Science robotics*, 2017.

[2] J. J. Abbott, E. Diller, and A. J. Petruska, "Magnetic methods in robotics," *Annual Review of Control, Robotics, and Autonomous Systems*, vol. 3, no. 1, pp. 57–90, 2020.

[3] S. Yim and M. Sitti, "Design and rolling locomotion of a magnetically actuated soft capsule endoscope," *IEEE Transactions on Robotics*, vol. 28, no. 1, pp. 183–194, 2011.

[4] C. Forbrigger, A. Lim, O. Onaizah, S. Salmanipour, T. Looi, J. Drake, and E. D. Diller, "Cable-less, magnetically driven forceps for minimally invasive surgery," *IEEE Robotics and Automation Letters*, vol. 4, no. 2, pp. 1202–1207, 2019.

[5] J. Pyrhönen, T. Jokinen, and H. Valéria, "Inductances," in *Design of Rotating Electrical Machines*. John Wiley & Sons, Ltd, p. 232.

[6] S. Sugimoto, "Current status and recent topics of rare-earth permanent magnets," *Journal of Physics D: Applied Physics*, vol. 44, no. 6, p. 064001, 2011.

[7] T. H. Boyer, "The force on a magnetic dipole," *American Journal of Physics*, vol. 56, no. 8, pp. 688–692, 1988.

[8] J. D. Jackson, "5.6 magnetic fields of a localized current distribution, magnetic moment," in *Classical electrodynamics*. American Association of Physics Teachers, vol. 2.

[9] M. P. Kummer, J. J. Abbott, B. E. Kratochvil, R. Borer, A. Sengul, and B. J. Nelson, "Octomag: An electromagnetic system for 5-dof wireless micromanipulation," *IEEE Transactions on Robotics*, vol. 26, no. 6, pp. 1006–1017, 2010.

[10] R. Zhang, S. Wu, Q. Ze, and R. Zhao, "Micromechanics study on actuation efficiency of hard-magnetic soft active materials," *Journal of Applied Mechanics*, vol. 87, no. 9, 2020.

[11] S. Erni, S. Schürle, A. Fakhraee, B. E. Kratochvil, and B. J. Nelson, "Comparison, optimization, and limitations of magnetic manipulation systems," *Journal of Micro-Bio Robotics*, vol. 8, no. 3, pp. 107–120, 2013.

[12] A. J. Petruska and J. J. Abbott, "Optimal permanent-magnet geometries for dipole field approximation," *IEEE transactions on magnetics*, vol. 49, no. 2, pp. 811–819, 2012.

[13] P. Ryan and E. Diller, "Magnetic actuation for full dexterity microrobotic control using rotating permanent magnets," *IEEE Transactions on Robotics*, vol. 33, no. 6, pp. 1398–1409, 2017.

[14] W. Hu, G. Z. Lum, M. Mastrangeli, and M. Sitti, "Small-scale soft-bodied robot with multimodal locomotion," *Nature*, vol. 554, no. 7690, pp. 81–85, 2018.

[15] J. Nam, W. Lee, J. Kim, and G. Jang, "Magnetic helical robot for targeted drug-delivery in tubular environments," *IEEE/ASME Transactions on Mechatronics*, vol. 22, no. 6, pp. 2461–2468, 2017.

[16] J. Leclerc, H. Zhao, D. Bao, and A. T. Becker, "In vitro design investigation of a rotating helical magnetic swimmer for combined 3-d navigation and blood clot removal," *IEEE Transactions on Robotics*, vol. 36, no. 3, pp. 975–982, 2020.

[17] D. Son, H. Gilbert, and M. Sitti, "Magnetically actuated soft capsule endoscope for fine-needle biopsy," *Soft robotics*, vol. 7, no. 1, pp. 10–21, 2020.

[18] G. Ciuti, P. Valdastri, A. Menciassi, and P. Dario, "Robotic magnetic steering and locomotion of capsule endoscope for diagnostic and surgical endoluminal procedures," *Robotica*, vol. 28, no. 2, pp. 199–207, 2010.

[19] G. Dogangil, O. Ergeneman, J. J. Abbott, S. Pané, H. Hall, S. Muntwyler, and B. J. Nelson, "Toward targeted retinal drug delivery with wireless magnetic microrobots," in *2008 IEEE/RSJ International Conference on Intelligent Robots and Systems*. IEEE, 2008, pp. 1921–1926.

[20] Y. Kim, E. Genevriere, P. Harker, J. Choe, M. Balicki, R. W. Regenhardt, J. E. Vranic, A. A. Dmytriw, A. B. Patel, and X. Zhao, "Telerobotic neurovascular interventions with magnetic manipulation," *Science Robotics*, vol. 7, no. 65, p. eabg9907, 2022.

[21] L. Leon, F. M. Warren, and J. J. Abbott, "Optimizing the magnetic dipole-field source for magnetically guided cochlear-implant electrode-array insertions," *Journal of medical robotics research*, vol. 3, no. 01, p. 1850004, 2018.

[22] M. Simi, G. Ciuti, S. Tognarelli, P. Valdastri, A. Menciassi, and P. Dario, "Magnetic link design for a robotic laparoscopic camera," *Journal of Applied Physics*, vol. 107, no. 9, p. 09B302, 2010.

[23] J. Pokki, O. Ergeneman, S. Sevim, V. Enzmann, H. Torun, and B. J. Nelson, "Measuring localized viscoelasticity of the vitreous body using intraocular microprobes," *Biomedical microdevices*, vol. 17, no. 5, pp. 1–9, 2015.

[24] D. Kim, J. Park, H. H. Park, and S. Ahn, "Generation of magnetic propulsion force and torque for microrobot using wireless power transfer coil," *IEEE Transactions on Magnetics*, vol. 51, no. 11, pp. 1–4, 2015.

[25] O. Onaizah and E. Diller, "Tetherless mobile micro-surgical scissors using magnetic actuation," in *2019 International Conference on Robotics and Automation (ICRA)*. IEEE, 2019, pp. 894–899.

[26] C. Forbrigger, A. Schonewille, and E. Diller, "Tailored magnetic torsion springs for miniature magnetic robots," in *2021 IEEE International Conference on Robotics and Automation (ICRA)*. IEEE, 2021, pp. 7182–7188.

[27] X. Wang, M. Luo, H. Wu, Z. Zhang, J. Liu, Z. Xu, W. Johnson, and Y. Sun, "A three-dimensional magnetic tweezer system for intraembryonic navigation and measurement," *IEEE Transactions on Robotics*, vol. 34, no. 1, pp. 240–247, 2017.

[28] L. Zhang, J. J. Abbott, L. Dong, K. E. Peyer, B. E. Kratochvil, H. Zhang, C. Bergeles, and B. J. Nelson, "Characterizing the swimming properties of artificial bacterial flagella," *Nano letters*, vol. 9, no. 10, pp. 3663–3667, 2009.

[29] J. Ali, U. K. Cheang, J. D. Martindale, M. Jabbarzadeh, H. C. Fu, and M. Jun Kim, "Bacteria-inspired nanorobots with flagellar polymorphic transformations and bundling," *Scientific reports*, vol. 7, no. 1, pp. 1–10, 2017.

[30] J. Yu, L. Yang, and L. Zhang, "Pattern generation and motion control of a vortex-like paramagnetic nanoparticle swarm," *The International Journal of Robotics Research*, vol. 37, no. 8, pp. 912–930, 2018.

[31] Z. Chen, Y. Lin, G. Zheng, Y. Yang, Y. Zhang, S. Zheng, J. Li, J. Li, L. Ren, and L. Jiang, "Programmable transformation and controllable locomotion of magnetoactive soft materials with 3d-patterned magnetization," *ACS Applied Materials & Interfaces*, vol. 12, no. 52, pp. 58 179–58 190, 2020.

[32] J. Li, W. Ma, F. Niu, Y. T. Chow, S. Chen, B. Ouyang, H. Ji, J. Yang, and D. Sun, "Development of biocompatible magnetic microrobot transporter using 3d laser lithography," in *2016 IEEE International Conference on Advanced Intelligent Mechatronics (AIM)*. IEEE, 2016, pp. 739–744.

[33] Y. Alapan, U. Bozuyuk, P. Erkoc, A. C. Karacakol, and M. Sitti, "Multifunctional surface microrollers for targeted cargo delivery in physiological blood flow," *Science robotics*, vol. 5, no. 42, p. eaba5726, 2020.

[34] J. Zhang, Z. Ren, W. Hu, R. H. Soon, I. C. Yasa, Z. Liu, and M. Sitti, "Voxelated three-dimensional miniature magnetic soft machines via multimaterial heterogeneous assembly," *Science robotics*, vol. 6, no. 53, p. eabf0112, 2021.

[35] P. K. Gupta, P. S. Jensen, and E. de Juan, "Surgical forces and tactile perception during retinal microsurgery," in *International conference on medical image computing and computer-assisted intervention*. Springer, 1999, pp. 1218–1225.

[36] I. Kuru, B. Gonenc, M. Balicki, J. Handa, P. Gehlbach, R. H. Taylor, and I. Iordachita, "Force sensing micro-forceps for robot assisted retinal surgery," in *2012 Annual International Conference of the IEEE Engineering in Medicine and Biology Society*. IEEE, 2012, pp. 1401–1404.

[37] D. Schuster, L. B. Kratchman, and R. F. Labadie, "Characterization of intracochlear rupture forces in fresh human cadaveric cochleae," *Otology & neurotology*, vol. 36, no. 4, pp. 657–661, 2015.

[38] A. A. Sharp, A. M. Ortega, D. Restrepo, D. Curran-Everett, and K. Gall, "In vivo penetration mechanics and mechanical properties of mouse brain tissue at micrometer scales," *IEEE transactions on biomedical engineering*, vol. 56, no. 1, pp. 45–53, 2008.

[39] M. Khadem, C. Rossa, R. S. Sloboda, N. Usmani, and M. Tavakoli, "Mechanics of tissue cutting during needle insertion in biological tissue," *IEEE Robotics and Automation Letters*, vol. 1, no. 2, pp. 800–807, 2016.

[40] S. Greenish, V. Hayward, V. Chial, A. Okamura, and T. Steffen, "Measurement, analysis, and display of haptic signals during surgical cutting," *Presence: Teleoperators & Virtual Environments*, vol. 11, no. 6, pp. 626–651, 2002.

[41] G. Cesaretti, D. Botticelli, A. Renzi, M. Rossi, R. Rossi, and N. P. Lang, "Radiographic evaluation of immediately loaded implants supporting 2–3 units fixed bridges in the posterior maxilla: a 3-year follow-up prospective randomized controlled multicenter clinical study," *Clinical oral implants research*, vol. 27, no. 4, pp. 399–405, 2016.

[42] M. Griffin, Y. Premakumar, A. Seifalian, P. E. Butler, and M. Szarko, "Biomechanical characterization of human soft tissues using indentation and tensile testing," *JoVE (Journal of Visualized Experiments)*, no. 118, p. e54872, 2016.

[43] P. Jamdagni and Y.-B. Jia, "Robotic cutting of solids based on fracture mechanics and fem," in *2019 IEEE/RSJ International Conference on Intelligent Robots and Systems (IROS)*. IEEE, 2019, pp. 8252–8257.

[44] R. H. Soon, Z. Ren, W. Hu, U. Bozuyuk, E. Yildiz, M. Li, and M. Sitti, "On-demand anchoring of wireless soft miniature robots on soft surfaces," *Proceedings of the National Academy of Sciences*, vol. 119, no. 34, p. e2207767119, 2022.

[45] Y. Yang, J. Wang, L. Wang, Q. Wu, L. Ling, Y. Yang, S. Ning, Y. Xie, Q. Cao, L. Li *et al.*, "Magnetic soft robotic bladder for assisted urination," *Science Advances*, vol. 8, no. 34, p. eabq1456, 2022.

[46] Q. Wang, K. F. Chan, K. Schweizer, X. Du, D. Jin, S. C. H. Yu, B. J. Nelson, and L. Zhang, "Ultrasound doppler-guided real-time navigation of a magnetic microswarm for active endovascular delivery," *Science advances*, vol. 7, no. 9, p. eabe5914, 2021.

[47] S. Koppoju, V. Chandrasekaran, and R. Gopalan, "52.7 koe high coercivity in sm (co0. 9cu0. 1) 4.8 melt-spun ribbons," *AIP Advances*, vol. 5, no. 7, p. 077118, 2015.

[48] Y. Huang, Z. Liu, X. Zhong, H. Yu, and D. Zeng, "Ndfeb based magnets prepared from nanocrystalline powders with various compositions and particle sizes by spark plasma sintering," *Powder metallurgy*, vol. 55, no. 2, pp. 124–129, 2012.

[49] K. Su, Z. Liu, H. Yu, X. Zhong, W. Qiu, and D. Zeng, "A feasible approach for preparing remanence enhanced ndfeb based permanent magnetic composites," *Journal of Applied Physics*, vol. 109, no. 7, p. 07A710, 2011.

[50] G. Chatzipirpiridis, O. Ergeneman, J. Pokki, F. Ullrich, S. Fusco, J. A. Ortega, K. M. Sivaraman, B. J. Nelson, and S. Pané, "Electroforming of implantable tubular magnetic microrobots for wireless ophthalmologic applications," *Advanced healthcare materials*, vol. 4, no. 2, pp. 209–214, 2015.

[51] J. Zhang, Y. Takahashi, R. Gopalan, and K. Hono, "Sm (co, cu) 5/ fe exchange spring multilayer films with high energy product," *Applied Physics Letters*, vol. 86, no. 12, p. 122509, 2005.

[52] H. Fujii and H. Sun, "Chapter 3 interstitially modified intermetallics of rare earth and 3d elements," in *Handbook of Magnetic Materials*. North-Holland Pub. Co., vol. 9, ISSN: 15672719 Publication Title: Ferromagnetic materials : a handbook on the properties of magnetically ordered substances.

[53] V. Panebianco, F. Giove, F. Barchetti, F. Podo, and R. Passariello, "High-field pet/mri and mrs: potential clinical and research applications," *Clinical and Translational Imaging*, vol. 1, no. 1, pp. 17–29, 2013.

[54] J. Rahmer, C. Stehning, and B. Gleich, "Remote magnetic actuation using a clinical scale system," *PloS one*, vol. 13, no. 3, p. e0193546, 2018.

[55] D. Li, M. Jeong, E. Oren, T. Yu, and T. Qiu, "A helical microrobot with an optimized propeller-shape for propulsion in viscoelastic biological media," *Robotics*, vol. 8, no. 4, p. 87, 2019.

[56] S. Park, B. Ko, H. Lee, and H. So, "Rapid manufacturing of micro-drilling devices using fff-type 3d printing technology," *Scientific Reports*, vol. 11, no. 1, pp. 1–9, 2021.

[57] C. Hong, Z. Ren, C. Wang, M. Li, Y. Wu, D. Tang, W. Hu, and M. Sitti, "Magnetically actuated gearbox for the wireless control of millimeter-scale robots,"*Science robotics* vol. 7, no. 69, p. eabo4401. 2022.

[58] M. M. Schmauch, S. R. Mishra, B. A. Evans, O. D. Velev, and J. B. Tracy, "Chained iron microparticles for directionally controlled actuation of soft robots," *ACS applied materials & interfaces*, vol. 9, no. 13, pp. 11 895–11 901, 2017.

[59] Y. Tang, M. Li, T. Wang, X. Dong, W. Hu, and M. Sitti, "Wireless miniature magnetic phase-change soft actuators," *Advanced Materials*, vol. 34, no. 40, p. 2204185, 2022.

[60] M. Li, Y. Tang, R. H. Soon, B. Dong, W. Hu, and M. Sitti, "Miniature coiled artificial muscle for wireless soft medical devices," *Science advances*, vol. 8, no. 10, p. eabm5616, 2022.

[61] O. Erin, X. Liu, J. Ge, J. Opfermann, Y. Barnoy, L. O. Mair, J. U. Kang, W. Gensheimer, I. N. Weinberg, Y. Diaz-Mercado *et al.*, "Overcoming the force limitations of magnetic robotic surgery: Magnetic pulse actuated collisions for tissue-penetrating-needle for tetherless interventions," *Advanced Intelligent Systems*, p. 2200072, 2022.

[62] Q. Wang, X. Du, D. Jin, and L. Zhang, "Real-time ultrasound doppler tracking and autonomous navigation of a miniature helical robot for accelerating thrombolysis in dynamic blood flow," *ACS nano*, vol. 16, no. 1, pp. 604–616, 2022.

[63] X. Wu, J. Liu, C. Huang, M. Su, and T. Xu, "3-d path following of helical microswimmers with an adaptive orientation compensation model," *IEEE Transactions on Automation Science and Engineering*, vol. 17, no. 2, pp. 823–832, 2019.

[64] T. Xu, C. Huang, Z. Lai, and X. Wu, "Independent control strategy of multiple magnetic flexible millirobots for position control and path following," *IEEE Transactions on Robotics*, 2022.

[65] J. Li, X. Li, T. Luo, R. Wang, C. Liu, S. Chen, D. Li, J. Yue, S.-h. Cheng, and D. Sun, "Development of a magnetic microrobot for carrying and delivering targeted cells," *Science Robotics*, vol. 3, no. 19, p. eaat8829, 2018.